

Design Analysis and Dynamic Modeling of a High-Speed 3T1R Pick-and-Place Parallel Robot

Guanglei Wu, Shaoping Bai and Preben Hjørnet

Abstract This paper introduces a four degree-of-freedom parallel robot producing three translation and one rotation (Schönflies motion). This robot can generate a rectangular workspace that is close to the applicable work envelope and suitable for pick-and-place operations. The kinematics of the robot is studied to analyze the workspace and the isocontours of the local dexterity over the representative regular workspace are visualized. The simplified dynamics is modeled and compared with Adams model to show its effectiveness.

Keywords Pick-and-place robots · Schönflies motion · Parallel manipulators · Dynamics

1 Introduction

The 3T1R (three translations and one rotation) robots have been widely used in material handling for pick-and-place operations. Compared to the serial SCARA robot, the parallel typed robots have the advantages in terms of high speed and light weight to improve productivity and reduce cost.

G. Wu (✉) · S. Bai
Department of Mechanical and Manufacturing Engineering,
Aalborg University, Aalborg, Denmark
e-mail: gwu@m-tech.aau.dk

S. Bai
e-mail: shb@m-tech.aau.dk

P. Hjørnet
Blue WorkForce A/S, Frederikshavn, Denmark
e-mail: ph@blueworkforce.com

Up to date, a number of parallel robots which can generate Schönflies motion have been presented. The successful Adept Quattro robot created by Pierrot and Company [1, 2], which has four symmetrical limbs, hit the market in 2007, is the fastest industrial robot available. It can accelerate at 200 m/s^2 with a 2 kg payload, being capable of moving 240 cycles per minute (cpm). By making use of the base structure of the Quattro robot, various robots with different mobile platforms have been introduced [3–5]. These robots usually have a cylindrical workspace. Besides, Angeles et al. proposed a two-limb 4-dof parallel manipulator to achieve high speed and a large workspace [6]. Recently, Angeles introduced the ‘pepper mill’ [7] robot with more simple structure.

This paper introduces a 3T1R parallel robot, which has a modified structure based on the Quattro robot. The design of this robot determines a rectangular workspace [8, 9] to allow more robots deployed above the conveyor, which is much more suitable for the pick-and-place application than the existing robots. The kinematics of the robot is developed and the workspace and dexterity are analyzed. Moreover, the dynamic model is established and illustrated with the standard testing trajectory, being validated by an Adams model.

2 Manipulator Architecture

The conceptual design of the new robot is shown in Fig. 1, whose motors are mounted at different orientations on the base frame, of which the axes of rotation are not coplanar. Each limb is composed of an inner arm and an outer arm (parallelogram, a.k.a ‘II joint’) connected to the base and mobile platforms.

The global coordinate frame xyz is built in Fig. 1b, whose origin is located at the geometric center of the base frame. The moving coordinate frame is attached to the mobile platform and the origin is at the geometric center. The geometric parameters of the first leg is displayed in the figure.

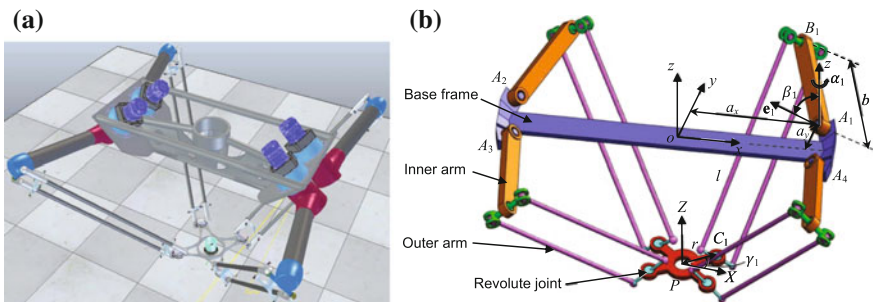


Fig. 1 The conceptual design of the robot: **a** CAD model, **b** schematic view

3 Mobility Analysis

The degree-of-freedom of the manipulator under study is derived by the Group Theory. The robot is composed of four $RR\Pi RR$ typed limbs as shown in Fig. 2 and the bond \mathcal{L}_i of the i th limb is the product of the following five bonds:

- The rotation subgroup $\mathcal{R}(\mathcal{A}_i)$ passing through A_i and parallel to \mathbf{e}_i .
- The rotation subgroup $\mathcal{R}(\mathcal{B}_i)$ passing through B_i and parallel to \mathcal{A}_i .
- The translation subgroup $\mathcal{T}(\mathbf{n}_i)$ corresponding to the Π -joint lying in a plane normal to \mathbf{n}_i .
- The rotation subgroup $\mathcal{R}(\mathcal{C}_i)$ passing through C_i and parallel to \mathcal{B}_i .
- The rotation subgroup $\mathcal{R}(\mathcal{C}'_i)$ passing through C_i and parallel to \mathbf{k} .

and \mathbf{k} is the unit vector of z -axis. Thus, the kinematic bonds of the i th limb is

$$\mathcal{L}_i = \mathcal{R}(\mathcal{A}_i) \cdot \mathcal{R}(\mathcal{B}_i) \cdot \mathcal{T}(\mathbf{n}_i) \cdot \mathcal{R}(\mathcal{C}_i) \cdot \mathcal{R}(\mathcal{C}'_i) \tag{1}$$

where the product of the first four bonds leads to the Schönflies group, namely,

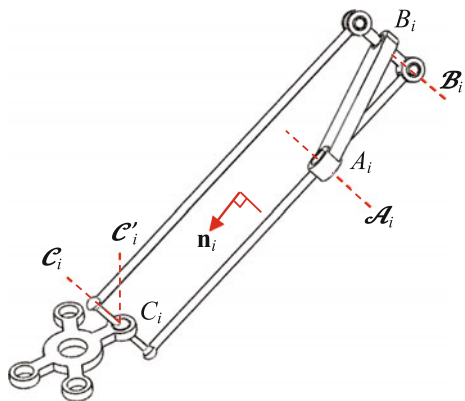
$$\mathcal{L}_i = \mathcal{X}(\mathbf{e}_i) \cdot \mathcal{R}(\mathcal{C}'_i) \equiv \mathcal{X}(\mathbf{k}) \cdot \mathcal{R}(\mathcal{C}_i) \tag{2}$$

Therefore, the intersection of the four limbs yields

$$\mathcal{L}_1 \cap \mathcal{L}_2 \cap \mathcal{L}_3 \cap \mathcal{L}_4 = \mathcal{X}(\mathbf{k}) \tag{3}$$

Henceforth, the intersection of all subgroups being a Schönflies subgroup $\mathcal{X}(\mathbf{k})$, the robot generates the Schönflies motion.

Fig. 2 The joints of the i th limb with rotation input



4 Kinematic Analysis of the Robot

Under the coordinate system depicted in Fig. 1b, the axis of rotation of the i th actuated joint is described by

$$\mathbf{e}_i = \mathbf{R}_i \mathbf{k}; \quad \mathbf{R}_i = \mathbf{R}(z, \alpha_i) \mathbf{R}(y, \beta_i) \mathbf{R}(z, \theta_i) \quad (4)$$

where $\alpha_{1(3)} = -\alpha_{2(4)} = \alpha$ and $-\beta_{1(4)} = \beta_{2(3)} = \pi/4$. Moreover, their position vectors in frame xyz are denoted by

$$\mathbf{a}_1 = -\mathbf{a}_3 = [a_x \ a_y \ 0]^T; \quad \mathbf{a}_2 = -\mathbf{a}_4 = [-a_x \ a_y \ 0]^T \quad (5)$$

then, the position vector of point B_i is derived as

$$\mathbf{b}_i = \mathbf{R}_i [b \ 0 \ 0]^T + \mathbf{a}_i \quad (6)$$

Let the mobile platform (MP) pose be denoted by $\mathbf{x} = [\mathbf{p}^T \ \phi]^T$, $\mathbf{p} = [x \ y \ z]^T$, the position vector of point C_i in frame xyz is expressed as

$$\mathbf{c}_i = \mathbf{Q} \mathbf{c}'_i + \mathbf{p} \quad (7)$$

where $\mathbf{Q} = \mathbf{R}(z, \phi)$ is the rotation matrix of the mobile platform and \mathbf{c}'_i is the position vector of C_i in the frame XYZ :

$$\mathbf{c}'_i = r [\cos \gamma_i \ \sin \gamma_i \ 0]^T; \quad \gamma_1 = -\gamma_4 = \gamma, \gamma_{2(3)} = \pi \mp \gamma \quad (8)$$

4.1 Inverse Geometric Problem

The inverse geometry problem is solved from the following kinematic constraints:

$$\|\mathbf{c}_i - \mathbf{b}_i\|^2 = l^2, \quad i = 1, \dots, 4 \quad (9)$$

Expanding and simplifying the above equation leads to

$$I_i \sin \theta_i + J_i \cos \theta_i + K_i = 0 \quad (10)$$

with

$$I_i = 2b(\mathbf{c}_i - \mathbf{a}_i)^T \mathbf{u}_i; \quad \mathbf{u}_i = [\sin \alpha_i \ \cos \alpha_i \ 0]^T \quad (11a)$$

$$J_i = -2b(\mathbf{c}_i - \mathbf{a}_i)^T \mathbf{v}_i; \quad \mathbf{v}_i = [\cos \alpha_i \ \cos \beta_i \ \sin \alpha_i \ \cos \beta_i \ -\sin \beta_i]^T \quad (11b)$$

$$K_i = \|\mathbf{c}_i - \mathbf{a}_i\|^2 + b^2 - l^2 \quad (11c)$$

Consequently, the inverse geometry problem is solved as

$$\theta_i = 2 \tan^{-1} \frac{-I_i \pm \sqrt{I_i^2 + J_i^2 - K_i^2}}{K_i - J_i} \quad (12)$$

From Eq. (12), it is seen that each limb has two solutions corresponding to two working modes. Here, the “- + -+” mode is selected as the working mode.

4.2 Kinematic Jacobian Matrix

Differentiating the four equations in Eq. (9) with respect to time yields

$$\mathbf{A}\dot{\mathbf{x}} = \mathbf{B}\dot{\boldsymbol{\theta}} \quad (13)$$

with

$$\mathbf{A} = [\mathbf{j}_1 \ \mathbf{j}_2 \ \mathbf{j}_3 \ \mathbf{j}_4]^T; \quad \dot{\mathbf{x}} = [\dot{x} \ \dot{y} \ \dot{z} \ \dot{\phi}]^T \quad (14a)$$

$$\mathbf{B} = \text{diag}[h_1 \ h_2 \ h_3 \ h_4]; \quad \dot{\boldsymbol{\theta}} = [\dot{\theta}_1 \ \dot{\theta}_2 \ \dot{\theta}_3 \ \dot{\theta}_4]^T \quad (14b)$$

where \mathbf{A} and \mathbf{B} are the forward and backward Jacobians, respectively, and

$$\mathbf{j}_i = [(\mathbf{c}_i - \mathbf{b}_i)^T (\mathbf{k} \times (\mathbf{c}_i - \mathbf{p}))^T (\mathbf{c}_i - \mathbf{b}_i)]^T \quad (15a)$$

$$h_i = (\mathbf{e}_i \times (\mathbf{b}_i - \mathbf{a}_i))^T (\mathbf{c}_i - \mathbf{b}_i) \quad (15b)$$

The kinematic Jacobian matrix is obtained as

$$\mathbf{J} = \mathbf{A}^{-1}\mathbf{B} \quad (16)$$

4.3 Workspace and Dexterity

The workspace (WS) can be found through the geometrical approach reported in [5] and visualized as shown in Fig. 3a, which admits a cuboid workspace. The corresponding geometric parameters are listed in Table 1. By changing the motor position and orientation, the robot topology can formulate workspace of different shapes, such as cylinder/trapezoid displayed in Fig. 3b, c.

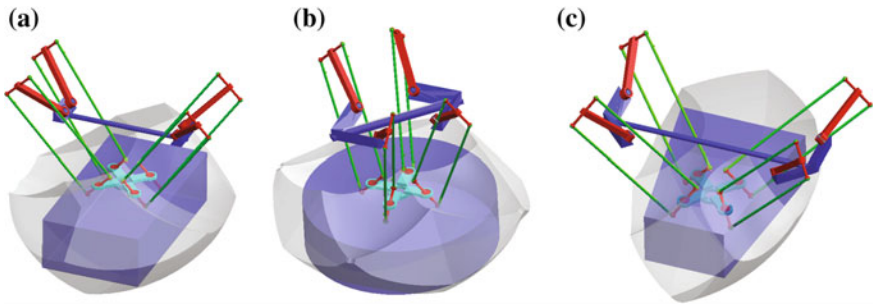


Fig. 3 Robot topologies with different shaped workspace

Table 1 Geometrical parameters of the robot

$[a_x, a_y]$ (mm)	α	b (mm)	l (mm)	r (mm)	γ
[200, 55]	15°	315	596	112	30°

Here, the cuboid WS in Fig. 3a will be investigated. As the the top view of the reachable WS has the cross-section close to superellipse, a superellipsoid is adopted to approximate the WS. Figure 4 shows the maximum superellipsoid workspace.

Dexterity is an utmost important concern, which is usually evaluated by the condition number of the kinematic Jacobian matrix. The entries of the forward Jacobian matrix of the robot are not homogeneous as they contain mixed rotation and translation terms, for which the condition number is limited to indicate the kinematic performance. Here, the characteristic length is introduced to normalize the forward Jacobian matrix below [5]:

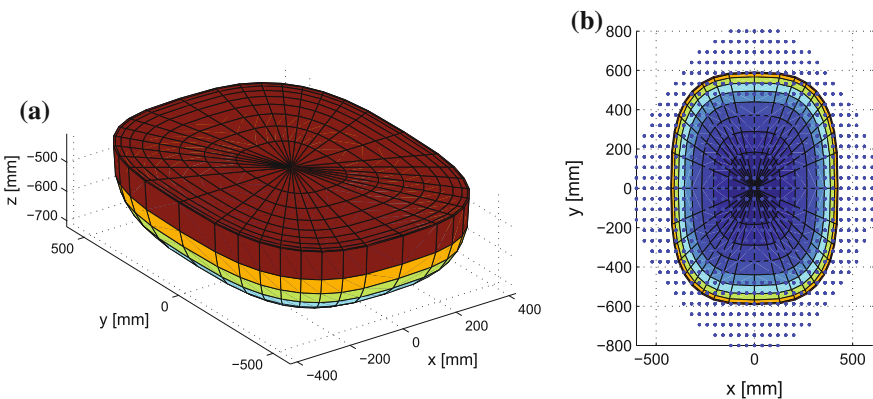


Fig. 4 The superellipsoid workspace with constant orientation $\phi = 0$: **a** 3D view, **b** top view

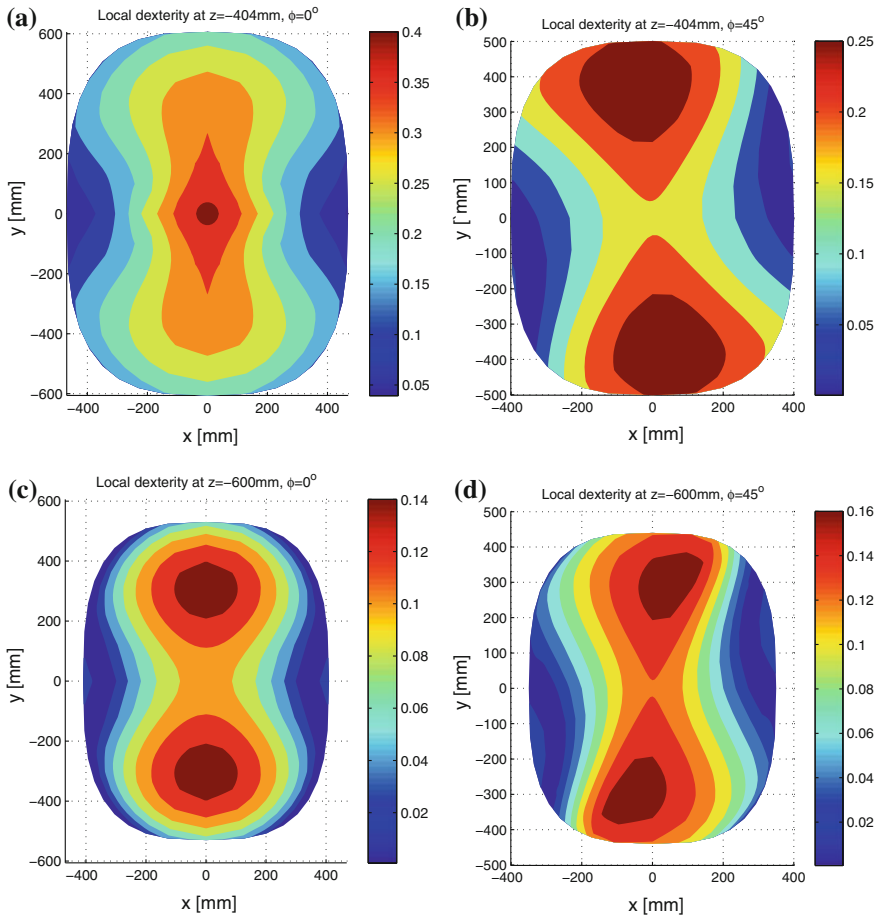


Fig. 5 Local dexterity distributions on *upper* and *lower* cross-sections of the workspace

$$L = \sqrt{\frac{3\mathbf{J}_\omega^T \mathbf{J}_\omega}{\text{tr}(\mathbf{J}_v^T \mathbf{J}_v)}} \tag{17}$$

where \mathbf{J}_v is the first three columns and \mathbf{J}_ω is the last one in \mathbf{A} , respectively, and then the forward Jacobian is normalized to $\mathbf{A}' = [\mathbf{J}_v/L \ \mathbf{J}_\omega]$. The local dexterity isocontours are displayed in Fig. 5, where the condition number is based on 2-norm. It is observed that the dexterous workspace nearly forms a rectangular volume that is suitable for pick-and-place operation.

5 Dynamic Modeling

Dynamics is used to compute the actuator torque/power, which is solved by using the Lagrange equations below

$$\frac{d}{dt} \left(\frac{\partial L}{\partial \dot{\mathbf{q}}} \right) - \frac{\partial L}{\partial \mathbf{q}} + \mathbf{C}_q^T \boldsymbol{\lambda} = \mathbf{Q}_{ex} \quad (18)$$

where $L \equiv T - V$ is the Lagrangian of the system, including the mobile platform and the four legs, and $\mathbf{q} = [\theta^T \mathbf{x}^T]^T$. Moreover, $\mathbf{Q}_{ex} = [\boldsymbol{\tau}^T, \mathbf{0}]^T \in \mathbb{R}^8$ is the vector of external forces and vector $\boldsymbol{\tau} = [\tau_1 \tau_2 \tau_3 \tau_4]^T$ characterizes the actuator torques. Matrix $\mathbf{C}_q = [\mathbf{B} - \mathbf{A}]$ is the system's constraint Jacobian. Moreover, $\boldsymbol{\lambda} = [\lambda_1 \lambda_2 \lambda_3 \lambda_4]^T$ is a vector of Lagrange multipliers.

In this modeling, the rotation of the outer arm is not considered for simplification, thus, the kinetic and potential energies are calculated below:

$$T = \sum_{i=1}^4 \left(\frac{1}{2} I_b \dot{\theta}_i^2 + \frac{1}{8} m_l (\dot{\mathbf{b}}_i + \dot{\mathbf{c}}_i)^T (\dot{\mathbf{b}}_i + \dot{\mathbf{c}}_i) + \frac{1}{2} m_j \dot{\mathbf{c}}_i^T \dot{\mathbf{c}}_i \right) + \frac{1}{2} \dot{\mathbf{x}}^T \mathbf{M}_p \dot{\mathbf{x}} \quad (19a)$$

$$V = \sum_{i=1}^4 \left(\frac{1}{2} m_b \mathbf{b}_i^T \mathbf{g} + \frac{1}{2} m_l (\mathbf{b}_i + \mathbf{c}_i)^T \mathbf{g} + m_j \mathbf{c}_i^T \mathbf{g} \right) + m_p \mathbf{p}^T \mathbf{g} \quad (19b)$$

where I_b and m_b are the moment of inertia and mass of the inner arm, respectively, and m_l , m_p and m_j are the masses of the outer arm, mobile platform and the joint on the latter. Moreover, $\mathbf{M}_p = \text{diag}[m_p \ m_p \ m_p \ I_p]$ is the mass matrix of the mobile platform. Terms $\dot{\mathbf{b}}_i$ and $\dot{\mathbf{c}}_i$ stand for the velocities of points B_i and C_i , respectively, which can be calculated with known $\dot{\theta}_i$ and $\dot{\mathbf{x}}$. In the above formulation, it is assumed that the centers of mass of the outer arms is coincident to their geometric centers.

Substituting Eq. (19) into Eq. (18), the terms in the equation of motion for this system can be derived. With payload \mathbf{f} , the actuator torques are expressed as:

$$\boldsymbol{\tau}_a = \boldsymbol{\tau} - \mathbf{J}^T \mathbf{f} \quad (20)$$

In order to evaluate the dynamic equation, a CAD model with geometrical parameters in Table 1 and mass properties in Table 2 was built in MSC Adams for comparison. The dynamic simulation is conducted with a pick-and-place trajectory of 25 mm × 305 mm × 25 mm, where the mobile platform positions in the y and z directions are shown in Fig. 6, and $x = 0$, $\phi = 0$, $\mathbf{f} = \mathbf{0}$.

The simulated velocity and acceleration profiles are shown in Fig. 7, where the solid and dashed lines stand for the Adams model and analytical model, respectively.

Table 2 The mass and moment of inertia of the robot for dynamic simulation

m_b (kg)	I_b (kg m ²)	m_l (kg)	m_j (kg)	m_p (kg)	I_p (kg m ²)
1.8	0.0595	0.42	0.2	2.2	0.026

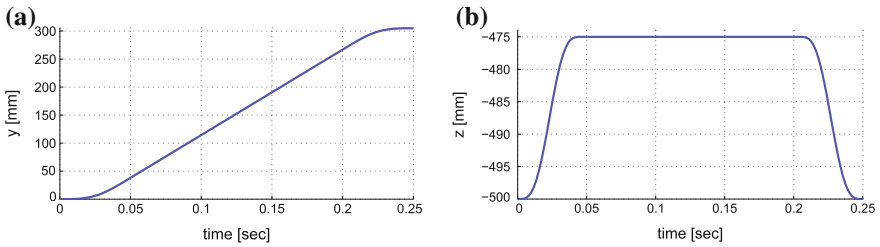


Fig. 6 The mobile platform positions with respect to time

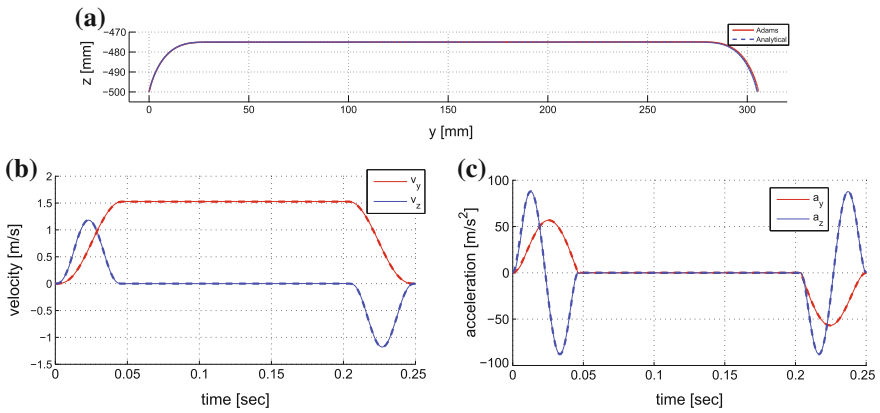


Fig. 7 Motion profiles of the testing trajectory for the Adams and analytical models

As a result, the motor torques and powers are illustrated with Fig. 8. It is noted that a gearbox with reduction ratio $\rho = 30$ is mounted on the output shaft in each limb. By comparison, it can be observed that there is a relatively good correlation between these two models.

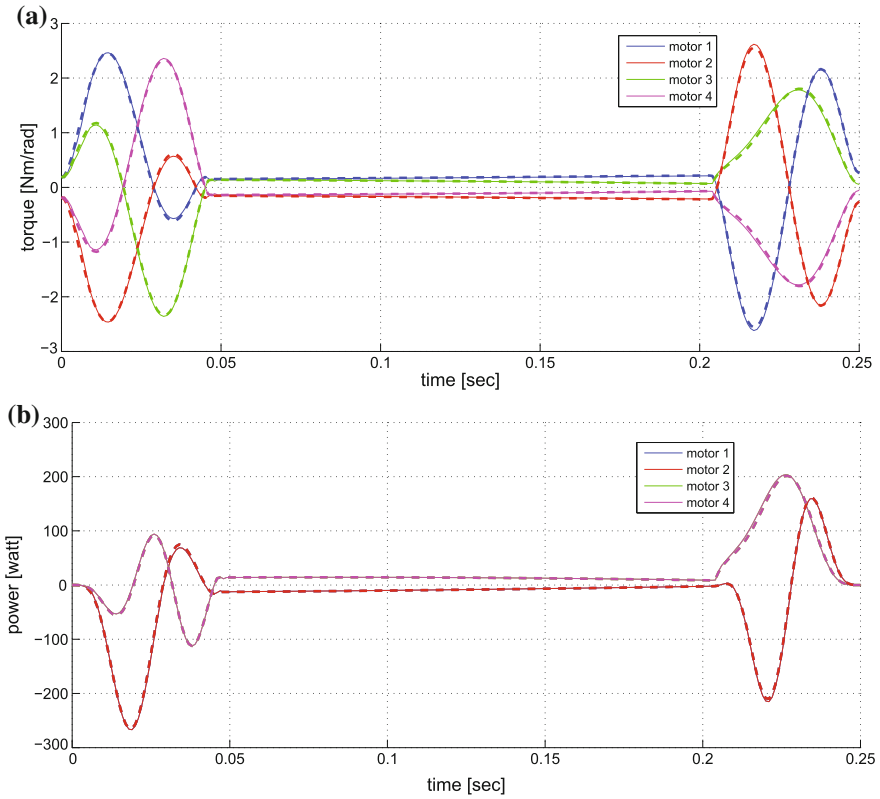


Fig. 8 The motor torques and powers along the testing trajectory

6 Conclusions

This paper introduces a 3T1R parallel robot, which can generate a rectangular workspace that is suitable for pick-and-place operations. The isocontours of the local dexterity distributions show that the robot can have a workspace with better kinematic performance to implement the pick-and-place operations. The simplified dynamic equations are modeled for the computation of motor torques and powers. Moreover, the dynamic model is validated with an Adams model.

Acknowledgments The authors would like to acknowledge Danish Innovationsfonden for the support under the Grant No. 137-2014-5.

References

1. Pierrot, F., et al.: H4: a new family of 4-dof parallel robots. In: IEEE/ASME International Conference on Advanced Intelligent Mechatronics, pp. 508–513 (1999)
2. Pierrot, F., et al.: Optimal design of a 4-DOF parallel manipulator: from academia to industry. *IEEE Trans. Robot.* **25**(2), 213–224 (2009)
3. Kong, X., et al.: Type synthesis of 3T1R 4-DOF parallel manipulators based on screw theory. *IEEE Trans. Robot. Autom.* **20**(2), 181–190 (2004)
4. Liu, S., et al.: Optimal design of a 4-DOF SCARA type parallel robot using dynamic performance indices and angular constraints. *J. Mech. Robot.* **4**(3), 031005 (2012)
5. Altuzarra, O., et al.: A symmetric parallel Schönflies-motion manipulator for pick-and-place operations. *Robotica* **29**(6), 853–862 (2011)
6. Cammarata, A., et al.: The dynamics of parallel schönflies motion generators: the case of a two-limb system, *Proceedings of the IMechE, Part I: J. Syst. Control Eng.* 223(11):29–52 (2009)
7. Harada, T., et al.: Kinematics and singularity analysis of a CRRHHRRC parallel Schönflies motion generator. *CSME Trans.* **38**(2), 173–183 (2014)
8. Bai, S., et al.: Design of a parallel robot with optimized workspace shape for fast and flexible pick-and-place operation. In: *Third IFToMM Asian-MMS*. Tianjin, China (2014)
9. Bai, S., et al.: Stiffness modeling of a 4-dof parallel robot for Schönflies motion generation. In: *ASME ESDA 2014*. Copenhagen, Denmark, ESDA2014-20094 (2014)